Hollow-Fiber Coating: Application to Preparation of Composite Hollow-Fiber Membrane for Gas Separation

Elsa Lasseuguette,[†,‡,§] Jean-Christophe Rouch,[†,‡] and Jean-Christophe Remigy*[,†,‡]

[†]Université de Toulouse, INPT, UPS, Laboratoire de Génie Chimique, 118 Route de Narbonne, F-31062 Toulouse, France
[‡]CNRS, Laboratoire de Génie Chimique, F-31030 Toulouse, France

ABSTRACT: Among the available membranes, dense polymer composite hollow-fiber membranes are promising for gas permeation applications coupled with the use of gas/liquid contactors, but they are also used in other membrane processes such as pervaporation. This study focuses on a coating process, starting from a polymer solution, to control the thickness and regularity of the coated polymer. The thickness of the liquid film coated onto a fiber is related to the coating velocity, the physical and chemical properties of the liquid, and the coating geometry. Depending on the dominating forces, several regimes are defined: two unstable regimes, in which a thin and regular polymer layer cannot be produced, and two stable regimes, which are of interest for reaching our objectives at the laboratory or industrial scale. The theoretical laws were compared to experimental coatings with solutions of poly(trimethylsilyl)propyne (PTMSP) dissolved in cyclohexane coated onto poly(ether sulfone) (PES) hollow fibers. The viscosities, surface tensions, and densities of the solutions used were measured. The experimental thicknesses of coated polymer layers were compared to values calculated from Landau's law, which describes the thickness behavior in the viscocapillary regime. The results showed good behavior agreement, but the experimental thickness was underestimated by the calculations. Four different kinds of composite membranes were prepared using two different porous supports (MicroPES and Oxyphan) and two different permeable polymers (PTMSP and Teflon AF2400) for coating. The obtained composites hollow fibers were characterized. All four presented low-energy surfaces with no wetting phenomena. They also exhibited high CO_2 and N_2 permeabilities with CO_2/N_2 selectivities between 3.4 and 2.5. The mechanical properties of the composites remained stable except for composites based on PES affected by the drying step during the coating process.

1. INTRODUCTION

Fiber coating processes are employed in many industries, for example, in the lubrication of glass or polymeric fibers, the protection of textile fibers, the coverage of conducting cable, or the development of composite fibers with two or more layers.

Membrane processes are an attractive emerging technology because of their high energy efficiency, compactness, and minimal environmental concerns. The membranes are porous or dense materials and can be found in flat or tubular geometries. In the latter case, they are called hollow fibers when the diameter is less than 1 or 2 mm. Membranes are usually used to filter water or to separate volatile components or gases. For gas separation and especially for CO_2 capture, the use of gas/liquid contactors based on microporous membranes is very efficient.[1−4] Such systems are more flexible and compact and less energy consuming. However, numerous limitations have been reported that might slow their use in industrial processes. The main issues with membrane technology are the wetting of the membrane, which increases the resistance to mass transfer and decreases the process efficiency,[5,6] and the limited long-term stability in terms of the chemical resistance of the membrane.[7] Luis et al.[2,3] outlined these limitations and identified the main challenges that still have to be solved to expand the use of membrane contactors in industry. Two approaches are considered to solve the wetting problem: improving the porous membrane or reducing the pore size to form a dense layer.

We focused our research on avoiding the wetting phenomenon by adding a dense polymer layer over a porous membrane. This approach is related to the densification of the membrane described by Luis et al.[2,3] Indeed, the goal is to physically separate the two phases using a highly permeable dense membrane without pores. The effectiveness of this approach was reported by Chabanon et al.[1] for CO_2 capture using a gas/liquid membrane contactor. Oxyphan fibers coated with Teflon AF2400 were put into contact with monoethanolamine solution for more than 1200 h. No wetting was noticed, and the efficiency of CO_2 capture was stable over time, in contrast to the observed behavior with virgin Oxyphan, where wetting occurred after only 200 h of experiments.

To obtain a high-performance membrane (high flux or productivity) using a dense membrane, the membrane should be very thin (i.e., micrometer range or less), but in this case, the mechanical resistance becomes very low. To avoid this problem, the use of composites is necessary. For instance, a new strategy based on composite hollow fibers, composed of a thin dense layer having high gas permeability and a macroporous support that provides favorable mechanical properties, has been developed. Composite membranes are already used in different applications such as pervaporation and gas perme-

ation. For example, Claes et al.[8] developed flat film supported poly(trimethylsilyl)propyne (PTMSP)−silica pervaporation membranes, and Yahaya[9] developed a composite hollow fiber with a dense layer of polydimethylsiloxane (PDMS) for the separation of volatile organic compounds (VOCs) from water. Sandru et al.[10] prepared composite membranes for gas permeation by coating poly(phenylene oxide) and polysulfone hollow fibers with a dense layer of poly(vinyl amine). These composite membranes were mainly made on the laboratory scale by dipping. We have developed a new method for the continuous coating of hollow fibers. The coating is obtained by a vertical coating process with the fiber rising from a liquid bath. The challenge was to obtain a uniform, thin, and regular coating to achieve the goals set for the dense composite hollow fibers such as high efficiency (i.e., gas permeability) without wetting problems. To our knowledge, this is the first time that optimum conditions for such a coating process have been studied.

This article focuses on the formation of a thin dense layer of polymer to produce a new composite hollow fiber for CO_2 capture. Applications for CO_2 capture by these membranes were reported in our previous work.[11] The dense layer was composed of a highly CO_2-permeable polymer, poly(trimethylsilyl)propyne (PTMSP) or Teflon AF2400. The support layer was a microporous hollow fiber of poly(ether sulfone) or polypropylene. It should be noted that the method described in this article could be applied to other polymers and membrane supports and, of course, to membrane processes that necessitate dense layers to be coated onto a hollow-fiber membrane. The objectives of this article are to report the continuous process conditions that were determined to obtain a uniform thin coating. After presenting the general theory of coating, we assess the efficiency of the composite membrane in terms of measurements of gas permeabilities, surface energies, and mechanical properties. Finally, the conditions required for coating PTMSP onto PES are analyzed more specifically and compared with calculated values.

2. MATERIALS AND METHODS

2.1. Materials. MicroPES and Oxyphan hollow fibers were purchased from Membrana GmbH (Wuppertal, Germany). Their characteristics are listed in Table S1 of the Supporting Information. Poly(trimethylsilyl)propyne (PTMSP) (M_n = 3 × 10^4 g mol^{-1}) was purchased from ABCR GmbH & Co. (Karlsruhe, Germany); it was purified before use by crystallization from methanol.[12] Teflon AF2400 (M_n unknown) was provided by Dupont de Nemours (Wilmington, DE). FluorinertFC72 was from 3M (St. Paul, MN). Other solvents were from Sigma-Aldrich (St. Louis, MO). All solvents were used as received without purification.

2.2. Solution Preparation. A given mass of PTMSP was dissolved in 100 g of solvent (cyclohexane for the coatings on MicroPES and chloroform for the coatings on Oxyphan). The mixture was stirred overnight to obtain a homogeneous solution. In the same way, Teflon AF2400 was dissolved in FluorinertFC72.

2.3. Analytical Techniques. The thickness of the composite fiber was examined by scanning electron microscopy (SEM; Hitachi TM1000, Tokyo, Japan). Fibers were first immersed in ethanol, cryofractured in liquid nitrogen, and then sputtered with a thin layer of gold. Deposit thickness was measured from the SEM image of a cross section. The viscosities of the solutions were measured at room temperature using a rheometer (Physica MCR301, Anton Paar GmbH, Graz, Austria) with a cone geometry (cone angle = 1°, diameter = 50 mm) and shear rate between 1 and 10^4 s^{-1}. The densities of the solutions were measured at 20 °C with a densitometer (30 PX, Metler Toledo, Viroflay, France). The surface tensions were measured at room temperature with a tensiometer (3S, GBX, Bourg de Peage, France) by using the Wilhelmy plate method. For contact angle determinations, 3-μL drops of water were placed on the hollow fibers, and the angles were measured with a goniometer (DiGiDrop Fast/60, GBX, Bourg de Peage, France). The surface energy of the hollow fibers was determined by measuring the contact angles of other liquids (diiodomethane, formamide) and following the classical approach proposed by Owens.[13] The fiber was positioned in the axis of the goniometer. As the volume of the drop was low and the fibers were hydrophobic, the curved surface of the fiber where the drop was placed can be considered as a flat surface.[14]

Water permeation was measured using poly(vinyl chloride) (PVC) modules made of 10 fibers with a length of around 20 cm. The water was fed into the outer side, and the operating pressure was slowly increased in steps of 0.5 bar up to 2 bar. At each pressure, a waiting time of at least 2 min was allowed to check whether water had permeated through to the lumen side. The water permeability measurements were normalized at 20 °C.[15] The lowest detectable water permeability was about 0.1 L h^{-1} bar^{-1} m^{-2}. This value was used to define a fiber that was nonpermeable toward liquid water.

The gas permeation of composite hollow fibers was measured using pure gases (CO_2, N_2). Laboratory-made stainless steel modules were used for the tests (Figure 1).

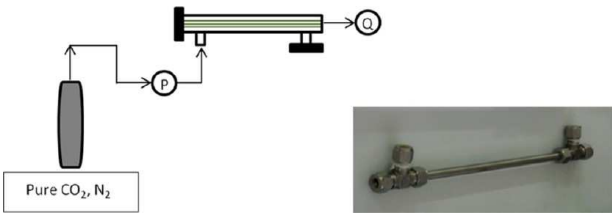

Figure 1. Setup for gas permeability experiments.

One or two fibers around 30 cm long were assembled in each module. The gas was fed into the shell side, and the gas permeation flux was measured at the outlet of the lumen side. The pressure was increased slowly in steps of 0.5 bar to 20 bar. Each measurement was recorded after 120 s of flux stabilization.

For a steady-state regime, the permeability [Lp(i)] of component i is calculated as

$$\mathrm{Lp}(i) = \frac{Q_{\mathrm{perm}}}{S(P_{\mathrm{feed}} - P_{\mathrm{perm}})} \quad (1)$$

where Q_{perm} is the flow rate of permeate (NL h^{-1}); P_{feed} and P_{perm} are the pressures (bar) of the feed and permeate parts, respectively; and S is the exchange surface area (m^2).

Thus, the selectivity of the membrane for component i relative to component j, $\alpha_{i,j}$, is defined as the ratio of the permeability coefficients of these components, that is

$$\alpha_{i,j} = \frac{\mathrm{Lp}(i)}{\mathrm{Lp}(j)} \quad (2)$$

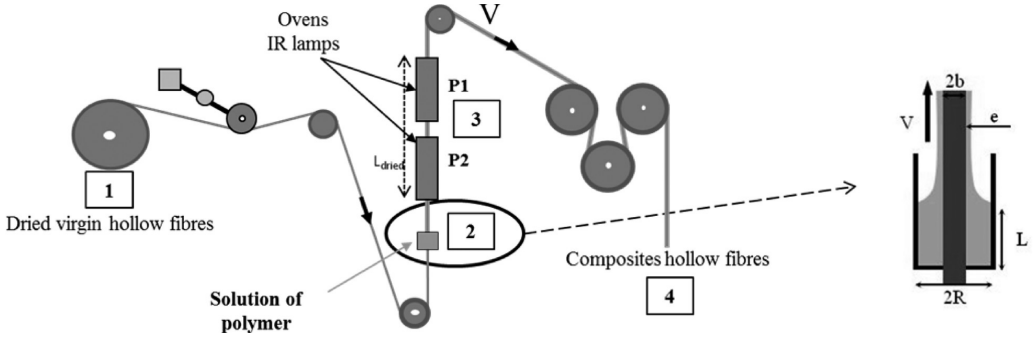

Figure 2. Schema of the hollow-fiber coating pilot and bath. R and L are the radius and length of the reservoir, respectively; b is the fiber radius (250 μm); and L_{dried} = 1.34 m.

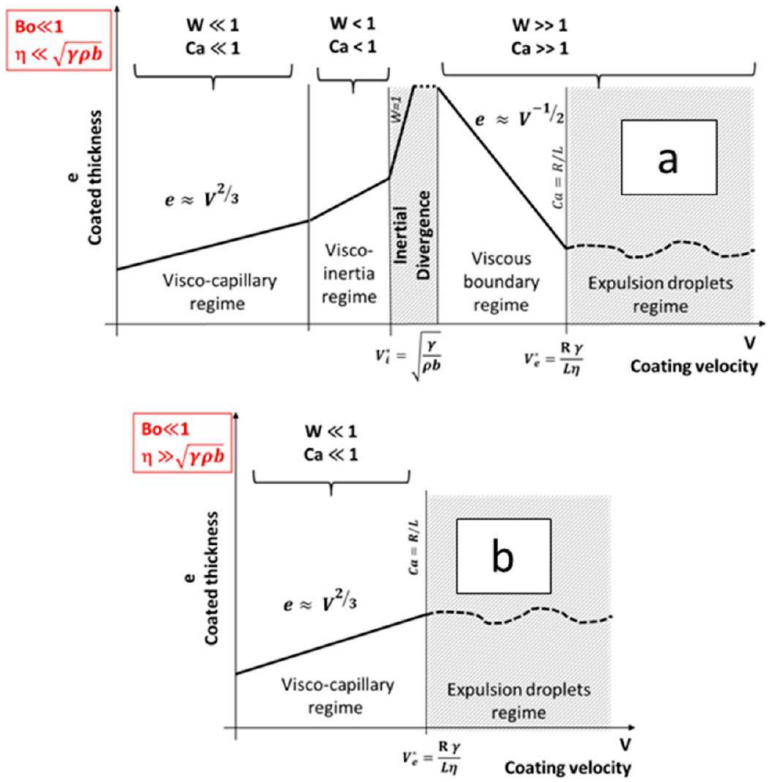

Figure 3. Coated liquid film thickness versus coating velocity with critical velocities.

2.4. Coating Setup. Composite fibers were obtained by formation of an outside coating of polymer solution followed by a drying step. The coating was prepared with a pilot setup developed in our laboratory using a continuous process (Figure 2). Dry virgin hollow fibers were coated directly without treatment (1). First, the virgin hollow fiber was passed through a solution of dissolved polymer (2) at room temperature. After the dip, a film of solution covered the fiber surface (Figure 2, right). Then, the fiber was dried (3) using two IR dryers (5.5 kW as electrical power, UVA Print LE with a Hg lamp and a glass filter, Honle UV, Bron, France) to evaporate the solvent.

The velocity of coating was changed from 4 to 18 m min^{-1}, leading to a residence time in the range of 1−20 s.

Several coatings were made with the two types of support and both types of dense layer (Table S2, Supporting Information).

2.5. Aging. Coated hollow fibers were aged for 6 months at room temperature and atmospheric pressure.

3. COATED LAYER THICKNESS

Landau and Levich[16] were the first to investigate the thickness of a Newtonian fluid coating on a fiber with a smooth surface. For small capillary numbers and negligible gravity, they showed that the film thickness is dependent on the coating velocity, the physical and chemical properties (viscosity and surface tension of the liquid), and the geometry of the fiber. Depending on the predominant forces, the thickness differs with the velocity.[17]

3.1. Viscocapillary Regime. When the Bond number, which compares gravity and capillary forces, as

$$Bo = \frac{\rho g b^2}{\gamma} \tag{3}$$

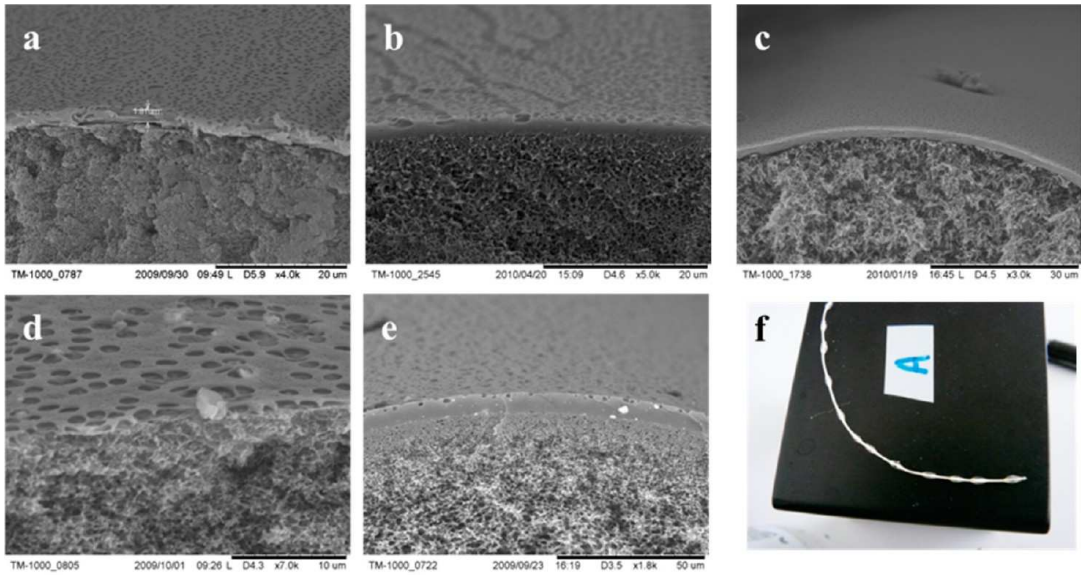

Figure 4. SEM cross sections of composite membranes: (a) Oxy_TF, (b) Oxy_PTMSP, (c) PES_TF, (d–f) PES_PTMSP.

is less than unity, gravity can be ignored. This also corresponds to the condition that the total thickness $(b + e)$ is much lower than the capillary length, $\kappa^{-1} = (\gamma/\rho g)^{1/2}$.

Thus, at low velocity, when capillary forces dominate over gravitational, inertial, and viscous forces, the Bond number and capillary number are well below 1. In this case, a viscous–capillary regime occurs. The thickness follows Landau's law

$$e = 1.34bCa^{2/3} \tag{4}$$

which indicates that the film thickness increases as a function of velocity to the power of $^2/_3$.

3.2. Inertia Divergence. When inertia is no longer negligible compared to capillary forces, the film thickness increases rapidly, and a divergence appears, called inertial divergence. This occurs when the velocity is higher than the critical velocity V_i^*

$$V_i^* = \sqrt{\frac{\gamma}{\rho b}} \tag{5}$$

Inertial divergence is not desirable owing to the fast growth of film thickness, which can lead to difficulties in controlling the uniformity of the thickness and also to overthick films.

3.3. Viscous Boundary Regime. When the velocity is high, a purely inertial regime exists. Capillary forces are negligible. In this case, the viscous boundary layer, formed along the fiber in the solution, is entrained by the fiber leaving the solution. The thickness follows the semiempirical formula

$$e = \alpha\sqrt{\frac{L\eta}{\rho V}} \tag{6}$$

where α is an experimental factor close to 1.

3.4. Expulsion Regime. An instability zone appears at the highest velocities when the viscous forces and inertia are predominant. In this zone, the viscous boundary layer affects the outside meniscus of the bath. As the viscous force (ηVL) exceeds the capillary force (γR), the meniscus twists, and a droplet is removed.[17] An expulsion regime appears with droplets expelled directly from the solution bath. By setting the two forces equal, one obtains a new critical velocity, V_e^*, where

$$V_e^* = \frac{R\gamma}{L\eta} \tag{7}$$

This expulsion regime is established as soon as the velocity is equal to V_e^* or the capillary number is equal to the geometric ratio R/L: $Ca = R/L$. The expulsion regime must be avoided because of the formation of droplets and irregular films. Stable thin films are obtained below this critical velocity.

3.5. Critical Velocities, Existence of Different Regimes, and Process Design. These different regimes are summarized in Figure 3 with arbitrarily set critical velocities.

For low viscosity, (Figure 3a), two stable regimes (viscocapillary or visco-inertial regime at low velocity and viscous boundary regime) and two unstable regimes (inertial divergence regime and expulsion regime) occur. Instabilities must be avoided to achieve well-controlled regular coatings.

For a given system (polymer solution and coating geometry), thin coatings, can be achieved at low velocity in the viscocapillary regime or at high velocity in the viscous boundary regime. For the latter, the extent is limited by the unstable expulsion regime. The viscocapillary regime is often used in the laboratory to make handmade composite membranes. To produce composite membranes on an industrial scale, high velocities are needed, and so the viscous boundary regime would be preferred. Therefore, it is necessary to push the expulsion regime limit (V_e^*) to high velocities. A high critical velocity V_e^* is achieved, for a given solution (fixed viscosity and surface tension), by designing the coating bath so that it has a high geometrical ratio R/L (large radius and small height). Thus, a short, wide solution bath must be used regardless of the solution properties. The same remarks can be made for high-viscosity solutions, except that the boundary regime and inertial divergence are never reached (Figure 3b). As soon as the viscous force exceeds the capillary force, the droplet expulsion regime occurs when $Ca = (\eta V)/\gamma > R/L$. The only way to produce a thin film is to operate the setup at low velocity, limiting the possibilities of industrial application.

Table 1. Characteristics of Composite Membranes

membrane	figure	concentration (w/w in solvent)	velocity (m min^{-1})	thickness (μm)	Lp(H_2O liquid)[a] (L h^{-1} m^{-2} bar^{-1})
Oxy_TF	Figure 4a	0.01	14.5	1.1	<0.1
Oxy_PTMSP	Figure 4b	0.01	7	1.9	<0.1
PES_TF	Figure 4c	0.01	14.5	1.4	<0.1
PES_PTMSP	Figure 4d	0.02	4	–	1400
	Figure 4e	0.05	6	2.7	<0.1
	Figure 4f	0.1	4	droplet	–

[a]Values at 20°C.

Thus, knowing the physical and chemical properties of the coated solution and the design of the process, it is possible to evaluate the coating velocities and the regions that could be used to avoid unstable regimes. However, these laws give the thickness of the solution layer before evaporation and not the final polymer film thickness. Assuming no polymer evaporation, polymer thickness depends on the polymer mass fraction in the coated solution and the thickness of the coated solution. As seen already, the thickness of the coated solution is a function of the velocity, the geometrical ratio R/L of the bath, and the physical and chemical properties of the coated solution (η, ρ, γ). The latter properties depend on the polymer mass fraction. Finally, the goal is to find the optimal set of parameters (velocity, geometrical ratio, polymer mass fraction) to obtain the desired polymer film thickness.

4. RESULTS

4.1. Dense Layer Characteristics. After each coating process had been completed, the membranes obtained were characterized by SEM. The surfaces and cross sections of the membranes were observed and the thickness was measured from SEM images. The operating conditions are listed in Table S2 of the Supporting Information, and selected SEM images are presented in Figure 4.

At low polymer mass fraction and low velocity, a nonuniform coating was obtained with holes appearing in the deposited layer (Figure 4d). This nonuniformity was confirmed by water permeability measurements (Table 1).

With an increase of polymer mass fraction, the coating thickness increased, and dense polymer films were obtained (Figure 4a–c,e). The surface of the coated layer did present craters, but the polymer layer remained intact, as confirmed by the absence of water permeability. At high mass fraction, droplets appeared along the fiber (Figure 4f).

4.1.1. Regularity of the Coating. The coating of Oxyphan with Teflon AF2400 was performed for an extended time. Figure 5 shows that the coating was regular over 1000 m of the fiber. The thickness presented few variations along the spool of the fiber. The average thickness was 1.15 μm with a standard deviation of 0.2.

4.1.2. Surface Energy. Water contact angle measurements are reported in Table 2. They show that the coating increased the hydrophobicity of the fibers. The surface energy of the composite hollow fibers was calculated using the Owens model[13] to obtain the dispersive and polar contributions.

From Table 2, it can be seen that the contact angle increased when a dense layer was added to the fibers, whereas the surface energy decreased, especially the polar component. Consequently, the composite hollow fibers were found to be highly hydrophobic materials.

4.2. Gas Permeability Coefficients and Selectivity. The pure-gas permeation (CO_2 and N_2) properties of composite hollow fibers are reported in Table 3 in terms of permeability coefficients and selectivities of CO_2 over N_2. All of the composite membranes were selective for CO_2, unlike the virgin

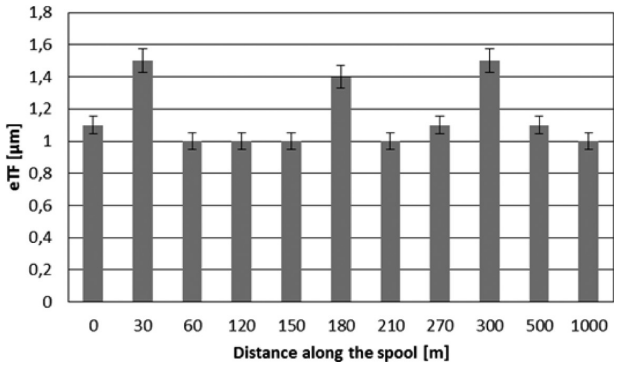

Figure 5. Thickness of the dense layer along the fiber spool.

Table 2. Surface Characteristics of Hollow-Fiber Composite

membrane	θ(H_2O) (deg, ±5°)	$\gamma_S = \gamma_p + \gamma_d$ (N m^{-1})
Oxyphan	110	11.8 = 1.2 + 10.6
Oxyphan_TF	127	5.6 = 0.5 + 5.1
Oxyphan_PTMSP	121	8.2 = 0.3 + 7.9
PES	82	37.9 = 37.7 + 0.2
PES_TF	127	5.6 = 0.5 + 5.1
PES_PTMSP	118	10.9 = 0.2 + 10.7

Table 3. Pure CO_2 and N_2 Permeability Coefficients and Selectivities of CO_2 over N_2 for the Composite Membranes

	e (μm)	Lp(CO_2)[a] (NL h^{-1} m^{-2} bar^{-1})	Lp(N_2)[b] (NL h^{-1} m^{-2} bar^{-1})	selectivity α_{CO_2/N_2}
PES_PTMSP	0.9	6772	–	–
	1.2	8442	2656	3.18 (±1.4)
	1.4	8000	–	–
	1.4	8915	–	–
	1.6	5588	1886	2.96 (±1.3)
	1.9	7304	2830	2.58 (±1.2)
	2.1	6673	1878	3.5 (±1.6)
	2.5	6250	–	–
	2.7	8458	–	–
PES_TF	0.9	9930	–	–
	1.6	6000	–	–
Oxyphan_PTMSP	1.9	3070	–	–
Oxyphan_TF	1.1	5120	1500	3.4 (±1.5)

[a]Accuracy error for Lp(CO_2 gas) = 16%. [b]Accuracy error for Lp(N_2 gas) = 26%.

fibers (Table S1, Supporting Information). Indeed, as Micro-PES and Oxyphan are microporous (average pore radius of 0.2 μm, values from Membrana), the transfer is convective without selectivity.[15]

For composite membranes, using the following model based on resistance in series

$$\frac{1}{\mathrm{Lp(AB)}} = \frac{1}{\mathrm{Lp(A)}} + \frac{1}{\mathrm{Lp(B)}} \quad (8)$$

where Lp is the permeability coefficient (NL h^{-1} m^{-2} bar^{-1}), A represents the virgin support, B represents the dense layer, and AB represents the composite membrane, it is possible to calculate the specific permeability of the dense layer and, thus, to determine its specific selectivity.

As Table 4 shows, the specific selectivities, α_{CO_2/N_2}, of the dense layers were similar to the values given in the literature.

Table 4. Specific Selectivities (α_{CO_2/N_2}) of the Dense Layers

dense layer	experimental	literature
PTMSP	3.3 (±0.6)	5.4[18]
		5.2[19]
		3.1[20]
Teflon AF2400	4 (±1.5)	5[21]
		4.4[22]

A variety of selectivity values have been reported for PTMSP. Indeed, the gas permeabilities of PTMSP membranes depend on the chemical structure of the polymer. For instance, this structure is greatly influenced by the nature of the catalysts used for the polymerization. Teplyakov et al.[19] showed that PTMSP synthesized with $TaCl_5$/Al(*i*-Bu)$_3$ presented a higher permeability than PTMSP prepared with $NbCl_5$. With $NbCl_5$, PTMSP had more cis structures, with a high-density physical network that induced a decrease in glassy matrix permeability. In the same way, the conditions for membrane elaboration, such as the solvent used and/or the velocity of the drying step, influence the ratio of cis/trans structures.[23]

4.2.1. Effect of Thickness. As expected, the gas permeability decreased with dense-layer thickness. Indeed, the presence of the dense layer leads to resistance to transfer. We noticed a decrease of around 90% of the permeability between the virgin fiber and the composite membrane.

However, the variation of the thickness had only a slight influence on permeability. Figure 6 shows that the permeability did not change dramatically with the thickness. The variations were within the error percentage instead of indicating a permeability decrease with increasing thickness.

The observations reported in Figure 6 are probably due to the different drying conditions used to make the different membranes. The dense layers of different thicknesses were not prepared in exactly the same way: the coating velocity and the PTMSP concentration differed. This means that the residence time changed and the IR energy received by the membrane changed as well.

As Figure 7 shows, we noticed that the permeability increased with the residence time. In fact, two phenomena occurred: First, the thickness of the coated polymer solution depends on the coating velocity: Under the conditions of Figure7, the thickness was low with a long residence time (i.e., a low coating velocity). This led to a thin, dense polymer layer after the complete evaporation of the solvent. Second, the gas

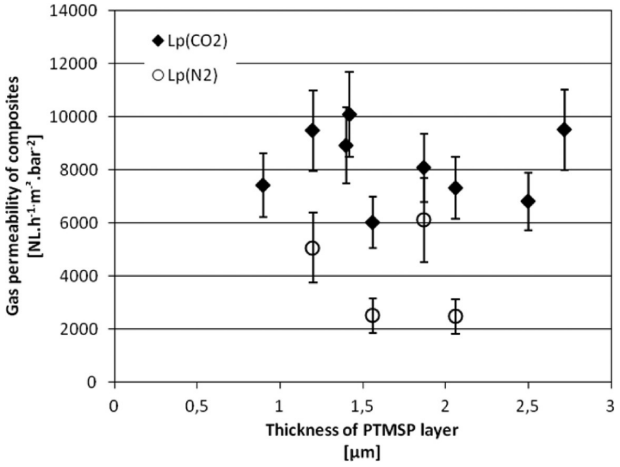

Figure 6. Variation of the permeability with the coating thickness (support, MicroPES; layer, PTMSP).

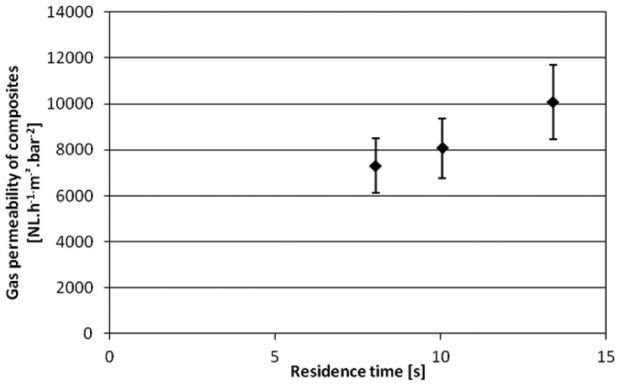

Figure 7. Variation of CO_2 permeability with residence time (support, MicroPES; layer, PTMSP; for [PTMSP] = 0.04).

permeability depends of the thickness of the dense layer: The permeability was high for a thin thickness.

For our system, for a slow drying step, the permeability coefficient was higher.

However, the permeability of PTMSP is known to change greatly with the operating conditions used for the elaboration of the membranes. The drying conditions[24,25] can influence polymer chain packing and, hence, gas permeability. Finally, Figure 6 indicates that the choice of drying conditions (solvent, evaporation rate, etc.) must also be taken into account to optimize the composite membrane when using a polymer having the same behavior than PTMSP. With Teflon AF, whose permeability depends less on operating conditions, the permeability increased with decreasing thickness.

4.2.2. Effect of Aging. In Table 5, we note the strong impact of the aging of PTMSP on gas permeability.

Table 5. Impact of Aging on the CO_2 Permeabilities of PTMSP and Teflon AF Layers

	Lp(CO_2) (barrer)	
dense layer	aged	fresh
PES_PTMSP, *e* (μm) = 1.56	3478	23460
PES_TF, *e* (μm) = 1. 6	3850	3905

After 6 months of physical aging, the gas permeability coefficient decreased by up to 85%. PTMSP appears to be sensitive to aging. The structure of the PTMSP polymer changes over time. A rearrangement of the physical structure occurs, as the polymer chains relax with a decrease of their free volumes.[23,27] As the permeability is related to the number of free volumes[25] by the equation

$$\mathrm{Lp} = K_1 \exp\left(-\frac{K_2}{\mathrm{FFV}}\right) \tag{9}$$

where Lp is the permeability of membrane (NL h^{-1} m^{-2} bar^{-1}), K_1 and K_2 are constants related to the structure of the membrane, and FFV is the number of free volumes, the permeability decreases.[23,26,28]

However, the composites with Teflon AF were stable with time. The permeability did not change for PES_TF. The chemical structure of perfluorinated materials is stable with time. Polyakov et al.[29] also noted that no reduction in permeation rates occurred even over a time frame of as much as 1 year for Teflon AF2400 membranes.

These results show that, for industrial applications, Teflon AF-coated membranes are better than PTMSP membranes because of their aging and permeability stability.

4.3. Mechanical Properties of Composites. The mechanical properties of the virgin porous support and coated hollow fibers are reported in Table 6.

Table 6. Mechanical Properties[a] of Virgin and Composite Fibers

	e (μm)	ε_B (%)	σ_B (MPa)	E (MPa)
Oxyphan	0	887	39.9	272
Oxyphan_TF	1.1	829	37.7	271
Oxyphan_PTMSP	1.9	497	26.8	265
MicroPES	0	60	6.6	108
PES_TF	0.9	33	6.3	141
PES_PTMSP	1.15	32.4	6.3	86
MicroPES + solvent + drying	0	33	5.5	82

[a] ε_B, elongation at break (%); σ_B, tensile strength (MPa); E, Young's modulus (MPa).

Table 6 indicates that coating caused a decrease of the breaking elongation, especially for MicroPES hollow fibers. The decrease of tensile properties of the composite based on PES is due only to the degradation of the support. We noticed a decrease of around 50% in elongation at the break point for MicroPES that passed through the pilot setup without receiving a polymer coating. The chemical structure of poly(ether sulfone) is affected by the drying step. Indeed, our IR dryers emitted UV radiation with wavelengths of >360 nm. Rivaton and Gardette[30] showed that photolysis at long wavelengths (λ > 300 nm) leads to chemical degradation with a cleavage of polymer chains. Chemical modification was confirmed by Fourier transform infrared (FTIR) analysis (Figure 8).

In a spectrum of dried virgin fiber, new peaks can be noted at 1740 and 1030 cm^{-1} that correspond to the appearance of sulfonic acid due to the cleavage of the sulfone linkage.[30] The scission of the main chain of the polymer parallels a decrease of the elongation.

However, the Young's moduli with and without the coating were found to be very similar. Except for PES, the coatings did not compromise the mechanical resistance of the composite fibers.

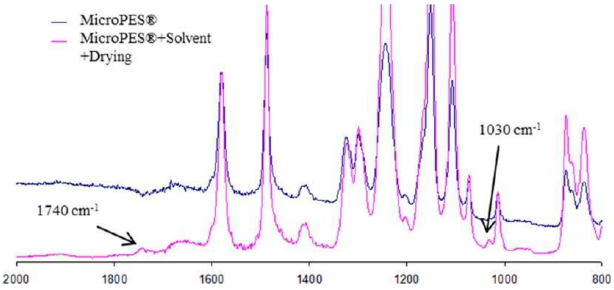

Figure 8. FTIR spectra of native MicroPES and dried MicroPES.

4.4. Experimental Results for Conditions of Coating. The conditions of the coating of PTMSP onto PES were analyzed more specifically and compared with the calculated values.

The experimental results are given in Table S2 of the Supporting Information.

4.4.1. Physical and Chemical Properties of PTMSP/Cyclohexane Solutions. The viscosities, surface tensions, and densities of the solutions used are reported in Table 7. The behaviors of viscosity, surface tension, and density with polymer mass fraction are presented in Figure 9. The solutions showed a shear-thinning behavior for shear rates between 1 and 1000 s^{-1}. For shear rates above 1000 s^{-1}, the viscosity was independent of the shear rate (Figure 9), and so, the solutions presented a Newtonian behavior.

For our coating experiments, the minimum shear rate was estimated at 10^4 s^{-1}. Therefore, we assumed that the solutions always behaved as Newtonian fluids. As a result, the values of the viscosity, given in Table 7, were recorded at a shear rate of 10^4 s^{-1}.

The increase of PTMSP mass fraction, [PTMSP], led to an increase of the viscosity and density with no change in the surface tension. The viscosity followed a classical experimental power law with the mass fraction of PTMSP

$$\eta = 11.984[\mathrm{PTMSP}]^{2.0676} \tag{10}$$

The density followed an increasing experimental linear law with the PTMSP mass fraction

$$\rho = 191.8[\mathrm{PTMSP}] + 778.8 \tag{11}$$

With eq 11, assuming ideal behavior, we estimated the density of pure PTMSP: ρ_{PTMSP} = 970 kg m^{-3}. This value is high with respect to literature values, which are around 750 kg m^{-3} for fresh PTMSP. However, Starannikova et al.[26] showed that, during physical aging, the density of PTMSP increases to 950 kg m^{-3}, a value in accordance with our extrapolation assuming ideal behavior.

As Table 7 shows, for all experiments, the Bond number was less than 1. Gravity was considered negligible. Moreover, the viscosity was always below the value of $(\gamma\rho b)^{1/2}$, except for solution 5. Therefore, for a mass fraction below 0.01 (w/w) PTMSP, the solutions used had low viscosities. As we saw in section 3.5, only the case a in Figure 3 could occur in the current experiments. For case b to occur, the solutions would have to have higher mass fractions.

4.4.2. Critical Velocities. Table 8 lists the critical velocities calculated using eqs 5 and 7 for each solution.

For all experiments except that involving solution 5, the critical expulsion velocity V_e^* was high in accordance with the earlier remarks on low-viscosity solutions. With our coating

Table 7. Properties of PTMSP Solutions in Cyclohexane

solution	[PTMSP] (w/w)	viscosity (at 10^4 s^{-1}) (Pa s)	surface tension (N m^{-1})	density (kg m^{-3})	Bond number (*Bo*)	$(\gamma\rho b)^{1/2}$
1	0.02	0.004	0.025	782	0.0192	0.067
2	0.03	0.007	0.025	784	0.0192	0.067
3	0.04	0.015	0.025	786	0.0193	0.07
4	0.05	0.024	0.025	788	0.0193	0.07
5	0.1	0.1	0.025	798	0.0196	0.07

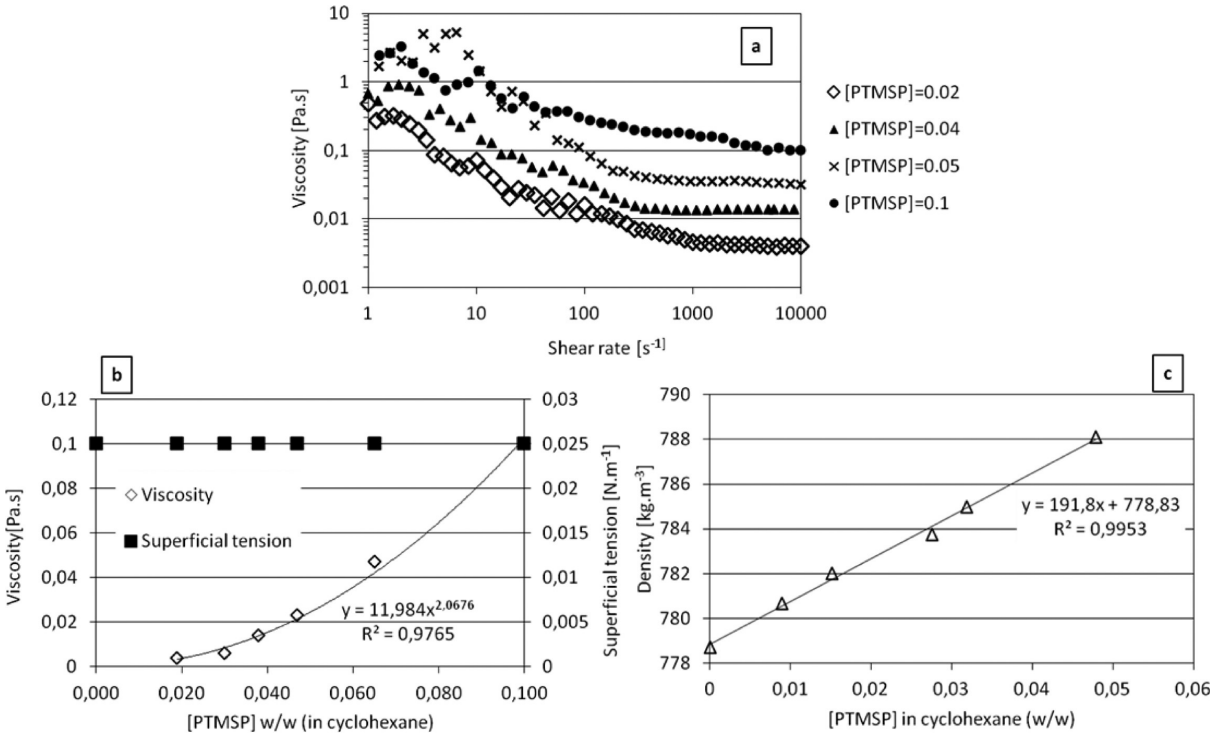

Figure 9. Physical and chemical properties of PTMSP solutions: (a) rheological behavior, (b) experimental viscosity (at 10^4 s^{-1}) and surface tension, and (c) density (the line plots the variation of the density versus the mass fraction).

Table 8. Critical Velocities of PTMSP Coatings[a]

solution	V_e^* (m min^{-1})	V_i^* (m min^{-1})
1	487	21.4
2	229	21.4
3	126	21.4
4	80	21.4
5	19	21.2

[a] R/L = 0.026/0.02 = 1.3.

setup, velocities higher than 40 m min^{-1} could not be achieved, so the expulsion regime never occurred. However, inertial divergence occurred at a velocity V_i^* close to 21 m min^{-1}.

For the high-mass-fraction solution, numbered 5 (i.e., [PTMSP] = 0.1 w/w), inertial divergence could not appear, and only the droplet expulsion regime occurred.

By plotting the determined critical velocities versus the PTMSP mass fraction (Figure 10), we determined a critical mass fraction above which the boundary layer regime could not occur.

As Figure 10 shows, the inertial critical velocity V_i^* is constant with the PTMSP mass fraction, whereas V_e^* decreases with increasing mass fraction. When the mass fraction exceeds the critical mass fraction X^*, the droplet expulsion regime

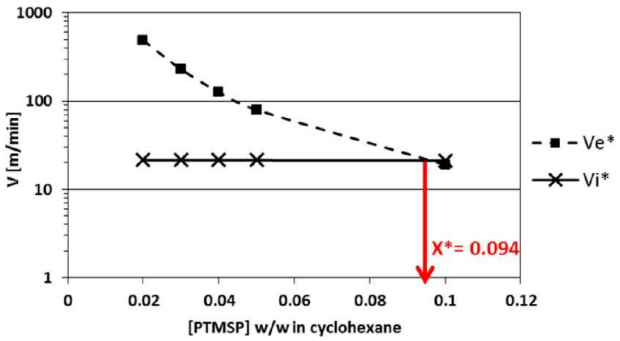

Figure 10. Critical velocities versus PTMSP mass fraction (R = 0.026 m, L = 0.02 m, and R/L = 1.3).

appears before the viscous boundary regime. The critical mass fraction indicates the maximum mass fraction for the onset of the boundary layer regime, which is interesting for industrial applications. It is important to note that this critical mass fraction depends on the geometry of the coating system and is therefore specific to the equipment used.

4.4.3. Calculated Coated PTMSP Thickness versus Experimental PTMSP Coated Thickness. In all cases, we assumed that the polymer did not evaporate whereas the solvent

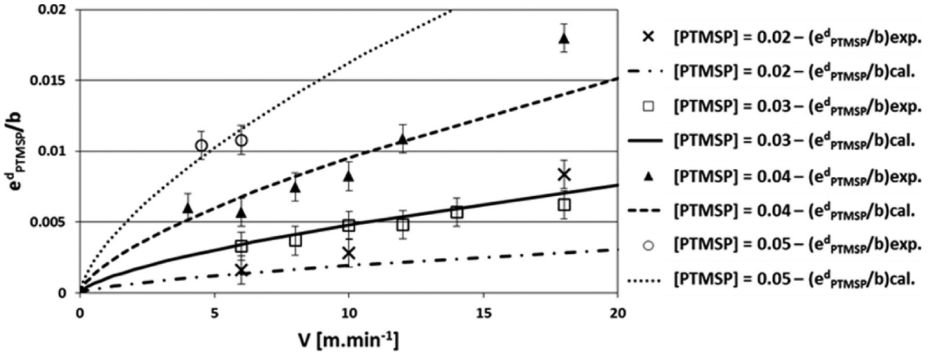

Figure 11. Behavior of calculated (lines) and experimental (points) dried film thickness normalized by the fiber radius (b = 250 μm) versus the coating velocity for different values of PTMSP mass fraction.

evaporated completely, so that the dried layer corresponds to a pure polymer layer. Assuming that the coated polymer has the same density as the neat polymer, the dried polymer thickness, e^d_{PTMSP}, was calculated from the liquid film thickness e according to the equation

$$e^d_{PTMSP} = e[PTMSP]\frac{\rho_{sol}}{\rho_{PTMSP}} \quad (12)$$

where ρ_{PTMSP} and ρ_{sol} are the densities of the polymer and of the coated solution, respectively.

The experiments were performed in the viscocapillary regime with negligible gravity. So, the liquid film thickness coated on the fiber was calculated using Landau's law (eq 4). The final polymer thickness is given by

$$e^d_{PTMSP} = 1.34b\left(\frac{\eta V}{\gamma}\right)^{2/3}[PTMSP]\frac{\rho_{sol}}{\rho_{PTMSP}} \quad (13)$$

Figure 11 compares the experimental polymer thickness with that calculated using eq 13. We can note a good fit for velocities below 15 m min^{-1}. Above 15 m min^{-1}, the experimental thickness was higher than that calculated. Indeed, at these velocities, the regime was close to inertial divergence with fast growth of the thickness, so that Landau's law was no longer valid. For solution 5 (i.e., [PTMSP] = 0.1), it was not possible to measure thickness accurately because of the droplets obtained even at low velocity.

Taking into account the low polymer mass fraction, the behavior of the physical and chemical properties can be obtained making the following assumptions:

- Surface tension is constant and equal to γ.
- The density follows the experimental linear law $\rho = k_\rho[PTMSP] + \rho_0$.
- The viscosity follows the experimental power law $\eta = \eta_0[PTMSP]^\beta$.

By combining these assumptions with Landau's law, the polymer thickness can be calculated from the mass fraction and the withdrawal velocity. These are the two practical parameters that must be chosen

$$e^d_{PTMSP} = b\frac{1.34}{\rho_{PTMSP}}\left(\frac{\eta_0 V}{\gamma}\right)^{2/3}(k_\rho[PTMSP]^{(2+2\beta/3)} + \rho_0[PTMSP]^{(1+2\beta/3)}) \quad (14)$$

Using experimental eqs 10 and 11, the thicknesses of the polymer layers were calculated and compared to the experimental thicknesses as shown in Figure 12. The

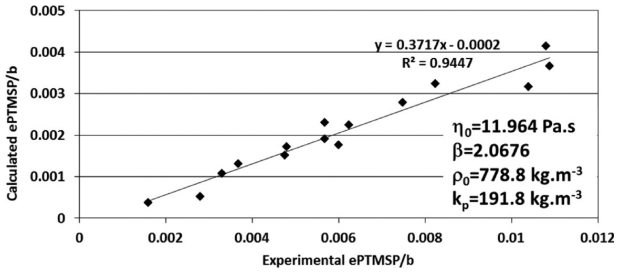

Figure 12. Calculated versus experimental ratio of the polymer thickness to the fiber radius.

correlation between the calculated and experimental thicknesses is good. However, the calculation underestimated polymer thickness by a factor of 2.6 regardless of the experimental conditions. This was probably due to the membrane roughness, as Chen[31] and Krechetnikov and Homsy[32] showed experimentally. They explained that the liquid film thickness is always higher on a rough surface than the measured value on a smooth surface (assumption for the theory of Landau's law). Taking this difference into account , the following equation can be used to calculate the coated PTMSP thickness

$$e^d_{PTMSP} = 2.6\frac{5.231b}{\rho_{PTMSP}(\gamma)^{2/3}}(V)^{2/3}(191.8[PTMSP]^{(3.623)} + 778.8[PTMSP]^{(2.623)}) \quad (15)$$

4.4.4. Droplets. During the experiment, droplets were observed at high mass fraction and high velocities (Figure 4f, Table S2 of the Supporting Information). However, the experimental velocities of droplet appearance were not correlated with the calculated velocities V_e^* for droplet appearance, as droplets appeared far below the calculated velocities; however, the observations were qualitatively in accordance with the calculated trend (Table 9).

Another instability could be involved: Plateau–Rayleigh instability.[33] This instability also leads to the formation of droplets. Indeed, a liquid film on a fiber spontaneously destabilizes: the liquid surface undulates up to the formation of a string of droplets. This instability is driven by the geometry

Table 9. Velocities at Droplet Appearance

solution	V_e^* calc (m min^{-1})	$V_{\text{drop app}}$ expt (m min^{-1})
1	487	NV[a]
2	229	NV[a]
3	126	14
4	80	8
5	19	4

[a]NV = not visible.

of the surface (cylinder) and the surface tension of the liquid.[34] For a thickness e that is very small compared to the radius of the fiber, the characteristic time of growth of this instability is given by the equation[35]

$$\tau_0 = \frac{12\eta b^4}{\gamma e^3} \tag{16}$$

The characteristic time of growth can be calculated from the law giving the liquid thickness as reported in section 3. For weakly concentrated solutions in the viscocapillary regime, the thickness follows Landau's law, and the coated liquid thickness is small compared to the radius of the fiber. Therefore, τ_0 can be expressed as a function of the coating velocity

$$\tau_0 = \frac{12\eta b^4}{\gamma e^3} = \frac{12\eta b^4}{\gamma\left[1.34b\left(\frac{\eta V}{\gamma}\right)^{2/3}\right]^3} \approx 5b\frac{\gamma}{\eta}\frac{1}{V^2} \tag{17}$$

This instability should appear when the residence time τ of the fiber in the coating setup is higher than the characteristic time of growth τ_0, considering that the coated layer is dried and solid at the oven exit. The resident time τ is then written as $\tau = L_{\text{dried}}/V$, where V is the coating velocity and L_{dried} is the length over which the fiber becomes dry (i.e., the length of the two dryers). With our pilot setup, the value of L_{dried} is equal to 1.34 m (Figure 2).

The limit between stable and unstable situations is obtained when $\tau = \tau_0$. In this case, eq 17 becomes $\tau_0 \approx 5b(\gamma/\eta)(\tau_0^2/L_{\text{dried}}^2)$, which allows the characteristic time of growth to be calculated as a function of the oven length, $\tau_0 \approx 5b(\eta/\gamma)(L_{\text{dried}}^2/5b)$ and, consequently, the critical velocity $V_0 \approx (\gamma/\eta)(5b/L_{\text{dried}})$ that defines the limit between stability and droplet formation. The practical velocity V should be higher than V_0 to operate in a stable regime without Plateau–Rayleigh instability.

Table 10 shows that the characteristic time of growth τ_0 increases with the mass fraction as a consequence of the

Table 10. Values of τ_0 and V_0 According the Mass Fraction

solution	τ_0 (s)	V_0 (m min^{-1})
1	230	0.34
2	490	0.16
3	804	0.1
4	1406	0.06
5	5900	0.01

increase in the viscosity that stabilizes the liquid film. The calculated critical velocities V_0 are very low. Consequently, during coating with our setup, Plateau–Rayleigh instability never occurred. Thus, this mechanism cannot explain the difference between the experimental and calculated velocities for the appearance of droplets. The mechanism that experimentally leads to the formation of droplets remains unknown. The rheological behavior of the solution used (viscoelasticity properties) and the consequences for the instability should be investigated. Moreover, the shear-rate variations of the coating process should be also studied.

4.4.5. Optimal Conditions. Using the equations giving the liquid thickness (see section 3) in accordance with the predominant forces and the experimental laws for viscosity, density, and surface tension, one can calculate the polymer mass fraction and velocity that should be used to coat a regular, thin layer of polymer on a fiber. For our process producing a composite membrane for CO_2 capture, a dry polymer thickness of 1 μm is a good objective in terms of performance.[11] Considering the coating of PTMSP onto MicroPES fiber and a given geometry for the coating reservoir, two regimes, and thus two equations, must be considered depending on the line rate. For a low line rate, thin liquid layers were obtained for velocities below the critical velocities for inertial divergence. Then, Landau's law must be used, resulting in the expression

$$e^{\text{d}}_{\text{PTMSP}} = b\frac{1.34}{\rho_{\text{PTMSP}}}\left(\frac{\eta_0 V}{\gamma}\right)^{2/3}(k_\rho[\text{PTMSP}]^{(2+2\beta/3)} + \rho_0[\text{PTMSP}]^{(1+2\beta/3)})$$

This equation can be reduced to

$$e^{\text{d}}_{\text{PTMSP}} = b\frac{1.34}{\rho_{\text{PTMSP}}}\left(\frac{\eta_0 V}{\gamma}\right)^{2/3}(\rho_0[\text{PTMSP}]^{(1+2\beta/3)})$$

as the first term of the equation is experimentally negligible. Considering an objective of 1 μm, one can calculate the relation between the PTMSP mass fraction and the line rate as

$$[\text{PTMSP}] = 0.053V^{-0.28} \tag{18}$$

For a high line rate (above inertial divergence and below the droplet expulsion regime), eq 8 is used, and the following equation is used to calculate the PTMSP thickness

$$e^{\text{d}}_{\text{PTMSP}} = \frac{\alpha}{\rho_{\text{PTMSP}}}\sqrt{\frac{L\eta_0}{V}}(k_\rho[\text{PTMSP}]^{(2+\beta/2)} + \rho_0[\text{PTMSP}]^{(1+\beta/2)})^{1/2}$$

Again, this equation can be reduced to

$$e^{\text{d}}_{\text{PTMSP}} = \frac{\alpha}{\rho_{\text{PTMSP}}}\sqrt{\frac{L\eta_0}{V}}(\rho_0[\text{PTMSP}]^{(1+\beta/2)})^{1/2}$$

as its first term equation is experimentally negligible. Considering an objective of 1-μm thickness and a geometry with L = 0.02 m and R = 0.026 m, one can calculate the relation between the PTMSP mass fraction and the line rate as

$$[\text{PTMSP}] = 0.0034V^{0.245} \tag{19}$$

If the thickness objective changes, eqs 18 and 19 will be different. We calculated an example for three thicknesses and two coating geometries (Figure 13). The curves indicate that different pairs of operating parameters (mass fraction, velocity) can be selected to coat a hollow fiber with a given thickness of the PTMSP layer. The unstable regions are also plotted in Figure 13a showing the operating limits. The critical velocity V_e^* is also dependent on the polymer mass fraction and the velocity. By the same reasoning as previously, we obtain the equation

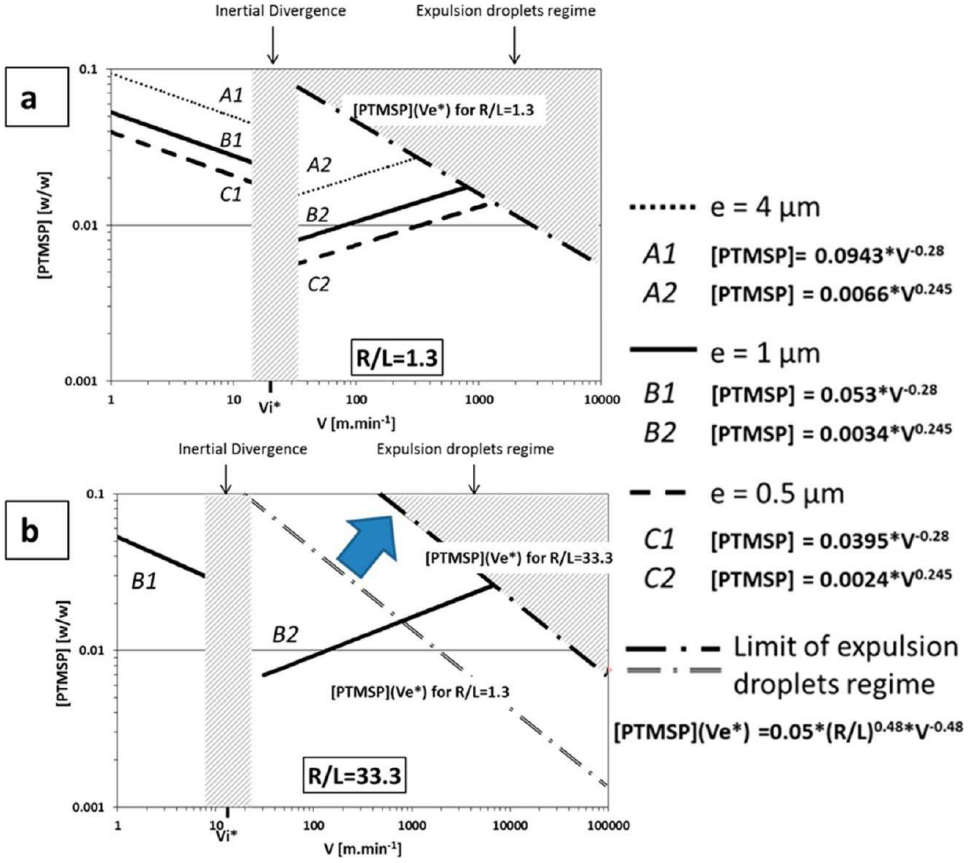

Figure 13. (a) Polymer mass fraction versus coating velocity for a thickness objective (e) of (A1,A2) 0.5, (B1,B2) 1, and (C1,C2) 4 μm, with R = 0.026 m and L = 0.02 m (R/L = 1.3). (b) Polymer mass fraction versus coating velocity for a thickness objective (e) of (B1,B2) 1 μm with R = 1 m, L = 0.03 m (R/L = 33.3) and R = 0.026 m, L = 0.02 m (R/L = 1.3). (Shared areas represent unstable conditions.)

$$[\mathrm{PTMSP}](V_e^*) = 0.05\left(\frac{R}{L}\right)^{0.48} V^{-0.48} \tag{20}$$

This equation gives the limit of the droplet expulsion regime. To change the coating thickness, either the velocity or the polymer mass fraction can be changed: For a given velocity, a higher mass fraction is required for a thicker coating.

Increasing the R/L ratio enlarges the boundary layer regime (i.e., right part of the graph), which allows the use of higher velocities.

For instance, in the textile industry, the typical velocity used for fiber lubrication is about 50 m s^{-1}, which is equivalent to 3000 m min^{-1}. Industrially, it is possible to obtain a 1-μm-thick coating on a fiber with a diameter of 500 μm. High velocity can be used with the mass fractions available here, as shown in Table 11.

Table 11. Selected Values of the Velocities and PTMSP Mass Fraction to Produce a 1-μm Coat of PTMSP on MicroPES Fiber[a]

velocity (m min^{-1})	[PTMSP] (w/w)
V_1 = 4	0.036
V_2 = 100	0.009
V_3 = 3000	0.021

[a] R = 1 m, L = 0.03 m, and R/L = 33.3.

Finally, the polymer coating thickness of a fiber taken from a liquid reservoir can be expressed easily with the coating velocity and the physical and chemical properties of the polymer solution.

5. CONCLUSIONS

Several hollow-fiber membrane composites were prepared using a new continuous coating process. The thickness of the coating on a fiber pulled through a reservoir of liquid polymer solution can be expressed easily in terms of the coating velocity and the physical and chemical properties of the polymer solution. Different coating regimes are defined depending on the dominant forces. The transitions between the regimes are defined by three critical velocities. Two regimes are unstable, such that regular thin films cannot be achieved, and must therefore be avoided. To obtain a thin layer of coating, two regimes are sought. The viscocapillary regime is used with a low velocity for experimental applications, whereas for use in industry, the high-velocity boundary layer regime is preferred. Velocity is limited by the droplet expulsion regime; its appearance depends on the geometry of the coating. The laws giving the thickness of the liquid coating depend on the polymer mass fraction of the coating solution and the velocity. Four composites were prepared with this new process. They showed good performance without wetting phenomena and high gas permeability. The composites coated with PTMSP proved sensitive to the process conditions and to aging. A slow

drying step led to high gas permeability, and with aging, the gas permeability decreased. In contrast for composites coated with Teflon AF, the permeability was stable. Finally, the coating of PTMSP solutions onto PES hollow fibers showed good agreement between the behavior of the calculated polymer coat thickness and thicknesses obtained during experiments performed in the viscocapillary regime.

ASSOCIATED CONTENT

Supporting Information

Characteristics of native fibers (Table S1), general conditions of coating (Table S2), and coating conditions and resulting coating thickness of PTMSP on MicroPES (Table S3). Cross section and surface of native fibers (MicroPES, Oxyphan) (Figure S1). This material is available free of charge via the Internet at http://pubs.acs.org.

AUTHOR INFORMATION

Corresponding Author

*Tel.: +33 561 557 618. Fax: +33 561 556 139. E-mail: remigy@chimie.ups-tlse.fr.

Present Address

[§]Scottish Carbon Capture and Storage Centre, Institute for Materials and Processes, School of Engineering, University of Edinburgh, Mayfield Road, Edinburgh EH9 3JL, U.K.

Notes

The authors declare no competing financial interest.

ACKNOWLEDGMENTS

This research was funded by the ANR (Agence Nationale de la Recherche) through funding of the Cicadi and AMELIE projects.

LIST OF SYMBOLS

b = fiber radius (m)
Bo = Bond number
Ca = capillary number
e = thickness of liquid film (m)
e^d = thickness of dried polymer (m)
L = reservoir length (m)
L_{dried} = length of two dryers (m)
[PTMSP] = mass fraction of PTMSP in cyclohexane
R = reservoir radius (m)
V = coating velocity (m s^{-1})
V^* = critical velocity (m s^{-1})
V_e^* = expulsion critical velocity (m s^{-1})
V_i^* = inertia critical velocity (m s^{-1})
W = Weber number
γ = superficial tension of the liquid (N m^{-1})
η = viscosity of the liquid (Pa s)
ρ = density of the liquid (kg m^{-3})
τ_0 = critical time of Plateau−Rayleigh instability (s)

REFERENCES

(1) Chabanon, E.; Roizard, D.; Favre, E. Membrane Contactors for Postcombustion Carbon Dioxide Capture: A Comparative Study of Wetting Resistance on Long Time Scales. *Ind. Eng. Chem. Res.* **2011**, *50*, 8237.

(2) Luis, P.; Van der Bruggen, B.; Van Gerven, T. Non-dispersive absorption for CO_2 capture: From the laboratory to industry. *J. Chem. Technol. Biotechnol.* **2011**, *86*, 769.

(3) Luis, P.; Van Gerven, T.; Van der Bruggen, B. Recent developments in membrane-based technologies for CO_2 capture. *Prog. Energy Combust. Sci.* **2012**, *38*, 419.

(4) Powel, C. E.; Qiao, G. G. Polymeric CO_2/N_2 gas separation membranes for the capture of carbon dioxide from power plant flue gases. *J. Membr. Sci.* **2006**, *279*, 1.

(5) Mavroudi, M.; Kaldis, S. P.; Sakellaropoulos, G. P. Reduction of CO_2 emissions by a membrane contacting process. *Fuel* **2003**, *82*, 2153.

(6) Wang, R.; Li, D. F.; Zhou, C.; Liu, M.; Liang, D. T. Impact of DEA solutions with and without CO_2 loading on porous polypropylene membranes intended for use as contactors. *J. Membr. Sci.* **2004**, *229*, 147.

(7) Atchariyawut, S.; Jiraratananon, R.; Wang, R. Separation of CO_2 from CH_4 by using gas−liquid membrane contacting process. *J. Membr. Sci.* **2007**, *304*, 163.

(8) Claes, S.; Vandezande, P.; Mullens, S.; De Sitter, K.; Peeters, R.; Van Bael, M. K. Preparation and benchmarking of thin film supported PTMSP-silica pervaporation membranes. *J. Membr. Sci.* **2012**, *389*, 265.

(9) Yahaya, G. O. Separation of volatile organic compounds (BTEX) from aqueous solutions by a composite organophilic hollow fibre membrane-based pervaporation process. *J. Membr. Sci.* **2008**, *319*, 82.

(10) Sandru, M.; Haubeko, S. H.; Hagg, M. Composite hollow fibre membranes for CO_2 capture. *J. Membr. Sci.* **2010**, *346*, 172.

(11) Nguyen, P. T.; Lasseuguette, E.; Medina-Gonzalez, Y.; Remigy, J. C.; Roizard, D.; Favre, E. A dense membrane contactor for intensified CO_2 gas/liquid absorption in post-combustion capture. *J. Membr. Sci.* **2011**, *377*, 261.

(12) Aouak, T.; Petit, A. Polymérisation des alcynes terminaux siliciés par un système amorceur constitué de carboxylate de Fe(III) et de triéthylaluminium: Synthèse et caractérisation. *Eur. Polym. J.* **1996**, *32*, 709.

(13) Owens, D. Some thermodynamic aspects of polymer adhesion. *J. Appl. Polym. Sci.* **1970**, *14*, 1725.

(14) Viswanadam, G.; Chase, G. C. Contact angles of drops on curved superhydrophobic surfaces. *J. Colloid Interface Sci.* **2012**, *367*, 472.

(15) Baker, R. W. *Membrane Technology and Applications*, 2nd ed.; John Wiley and Sons: Chichester, U.K., 2004.

(16) Landau, L.; Levich, B. Dragging of a liquid by a moving plate. *Acta Physicochim. USSR* **1942**, *17*, 42.

(17) Quéré, D.; de Ryck, A. Le mouillage dynamique d'une fibre. *Ann. Phys (Paris)* **1998**, *23*, 1.

(18) Pinnau, I.; Toy, L. G. Transport of organic vapors through poly(1-trimethysilyl-1-propyne). *J. Membr. Sci.* **1996**, *116*, 199.

(19) Teplyakov, V. V.; Roizard, D.; Favre, E.; Khotimsky, V. S. Investigations on the peculiar permeation properties of volatile organic compounds and permanent gases through PTMSP. *J. Membr. Sci.* **2003**, *220*, 165.

(20) T Merkel, T. C.; Gupta, R. P.; Turk, B. S.; B.D Freeman, B. D. Mixed-gas permeation of syngas components in poly(dimethylsiloxane) and poly(1-trimethylsilyl-1-propyne) at elevated temperatures. *J. Membr. Sci.* **2001**, *191*, 85.

(21) Pinnau, I.; Toy, L. G. Gas and vapor transport properties of amorphous perfluorinated copolymer membranes based on 2,2-bistrifluoromethyl-4,5-difluoro-1,3-dioxole/tetrafluoroethylene. *J. Membr. Sci.* **1996**, *109*, 125.

(22) T Merkel, T. C.; Pinnau, I.; Prabhakar, R.; Freeman, B. D. Gas and Vapor Transport Properties of Perfluoropolymers. In *Materials Science of Membranes for Gas and Vapor Separation*; Yampolskii, Y. P., Pinnau, I., Freeman, B. D., Eds.; John Wiley & Sons, Ltd.: New York, 2006; p 251.

(23) Nagai, K.; Masuda, T.; Nakagawa, T.; Freeman, B. D.; Pinnau, I. Poly[1-(trimethylsilyl)-1-propyne] and related polymers: Synthesis, properties and functions. *Prog. Polym. Sci.* **2001**, *26*, 721.

(24) Thomas, S.; Pinnau, I.; Du, N.; Guiver, M. Pure- and mixed-gas permeation properties of a microporous spirobisindane-based ladder polymer (PIM-1). *J. Membr. Sci.* **2009**, *333*, 125.

(25) Gomes, D.; Nunes, S. P.; Peinemann, K. V. Membranes for gas separation based on poly(1-trimethylsilyl-1-propyne)−silica nanocomposites. *J. Membr. Sci.* **2005**, *246*, 13.
(26) Starannikova, L.; Khodzhaeva, V.; Yampolskii, Y. Mechanism of aging of poly[1-(trimethylsilyl)-1-propyne] and its effect on gas permeability. *J. Membr. Sci.* **2004**, *244*, 183.
(27) Fujita, H. Notes on Free Volume Theories. *Polym. J.* **1991**, *23*, 1499.
(28) Morlière, N.; Vallières, C.; Perrin, L.; Roizard, D. Impact of thermal ageing on sorption and diffusion properties of PTMSP. *J. Membr. Sci.* **2006**, *270*, 123.
(29) Polyakov, A. M.; Starannikova, L. E.; Yampolskii, Y. P. Amorphous Teflons AF as organophilic pervaporation materials: Transport of individual components. *J. Membr. Sci.* **2003**, *216*, 241.
(30) Rivaton, A.; Gardette, J. L. Photodegradation of polyethersulfone and polysulfone. *Polym. Degrad. Stab.* **1999**, *66*, 385.
(31) Chen, J. D. Measuring the film thickness surrounding a bubble inside a capillary. *J. Colloid Interface Sci.* **1986**, *109*, 341.
(32) Krechetnikov, R.; Homsy, G. M. Experimental study of substrate roughness and surfactant effects on the Landau−Levich law. *Phys. Fluids* **2005**, *17*, 102.
(33) Plateau, J. *Statique expérimentale et théorique des liquides soumis aux seules forces moléculaires*; Gauthier-Villars: Paris, 1873.
(34) Quéré, D. Thin films flowing on vertical fibres. *Europhys. Lett.* **1990**, *13*, 721.
(35) De Gennes, P. G.; Brochard-Wyart, F.; Quéré, D. *Gouttes, Bulles, Perles et Ondes*; Collection Echelles; Belin: Paris, 2002.